PROGRESS IN PHOTOVOLTAICS: RESEARCH AND APPLICATIONS
Prog. Photovolt: Res. Appl. 2011; **19**:61–72
Published online 15 July 2010 in Wiley Online Library (wileyonlinelibrary.com). DOI: 10.1002/pip.988

RESEARCH ARTICLE

Four-junction spectral beam-splitting photovoltaic receiver with high optical efficiency

Bernhard Mitchell*, Gerhard Peharz, Gerald Siefer, Marius Peters, Tobias Gandy, Jan Christoph Goldschmidt, Jan Benick, Stefan W. Glunz, Andreas W. Bett and Frank Dimroth

Fraunhofer Institute for Solar Energy Systems, Heidenhofstrasse 2, 79110 Freiburg, Germany

ABSTRACT

A spectral beam-splitting architecture is shown to provide an excellent basis for a four junction photovoltaic receiver with a virtually ideal band gap combination. Spectrally selective beam-splitters are used to create a very efficient light trap in form of a 45° parallelepiped. The light trap distributes incident radiation onto the different solar cells with an optical efficiency of more then 90%. Highly efficient solar cells including III–V semiconductors and silicon were fabricated and mounted into the light trapping assembly. An integrated characterization of such a receiver including the measurement of quantum efficiency as well as indoor and outdoor I–V measurements is shown. Moreover, the optical loss mechanisms and the optical efficiency of the spectral beam-splitting approach are discussed. The first experimental setup of the receiver demonstrated an outdoor efficiency of more than 34% under unconcentrated sunlight. Copyright © 2010 John Wiley & Sons, Ltd.

KEYWORDS

high efficiency; multi-junction; spectral beam-splitting; dichroic mirror

***Correspondence**

Bernhard Mitchell, ARC Photovoltaics Centre of Excellence, University of New South Wales, Sydney 2052, Australia.
E-mail: bernhard.mitchell@gmail.com

Received 14 October 2009; Revised 4 March 2010

1. INTRODUCTION

The currently most successful approach to reach high photovoltaic conversion efficiency is to use multi-junction solar cells under concentrated sunlight. Multi-junction solar cells can convert the solar spectrum more efficiently than a single-junction solar cell by utilizing different semiconductor materials with appropriate band gap energies for different parts of the solar spectrum. Thus the multi-junction approach reduces thermalization and transmission losses, which yields to an increased efficiency maximum in comparison to a single-junction solar cell.

Multi-junction solar cell devices have been the subject of ongoing research over the past 20 years and started with the development of mechanically stacked dual-junction cells [1–3]. However, improvements in epitaxial growth led to efficient monolithically grown dual- and triple-junction solar cells [4–7]. The major constraint of the monolithic multi-junction solar cell approach is the current-matching constraint due to the series connection of the subcells, which leads to the loss of excess currents. The epitaxial growth usually also requires a good matching of the lattice constants, which limits the material and thus band gap selection. An approach to overcome this limitation is a geometrically spectrum-splitting architecture. This architecture incorporates several separate single- or dual-junction solar cells optimized for different parts of the solar spectrum, each suited to convert the corresponding part of the solar spectrum with the highest efficiency. The core components of the spectrum-splitting architecture are spectrally selective filters (beam-splitters), which are used to split the incident solar radiation and to direct the light towards the different solar cells. With this approach, the different solar cells can be individually designed without any constraints in current or lattice matching. Therefore, the architecture enables the combination of a broad range of materials can be used to design a highly efficient multi-junction photovoltaic receiver.

The light splitting approach to reach highly efficient photovoltaic conversion was first experimentally investigated in 1978 by Moon *et al.* [8] showing a 28.5% outdoor efficiency. They used a spectral beam-splitting arrangement with a 17-layer beam-splitter and assembled an AlGaAs and a Si solar cell. Ultra high efficiency approaches were discussed in Green [9] and Marti *et al.* [10]. A good review of spectral beam-splitting technologies is given by Imenes

et al. [11], who also discussed possible strategies to improve the spectral performance of interference filters used in photovoltaic devices [12]. The spectrum-splitting approach has been researched again due to developments in interference filter technology [13–18], which make the spectral beam-splitting approach more attractive.

In this paper, a spectrally selective filter-based beam-splitting receiver in a parallelepiped configuration is presented, which is designed to reach high solar electrical conversion efficiencies. At first, the parallelepiped arrangement and the theoretically optimized solar cell selection are presented. Subsequently, the methods used to characterize the beam-splitters and the full receiver setup, are described. Moreover, the results of the quantum efficiency measurements as well as indoor and outdoor efficiencies are shown. Additionally, the optical efficiency of the receiver including photon and the voltage losses are discussed. In conclusion, this work shows the full efficiency potential of the beam-splitting multi-junction approach in an experimental setup.

2. THE RECEIVER CONCEPT

The presented multi-junction receiver is based on the geometry of a parallelepiped (Figure 1). This configuration offers complete freedom in solar cell selection, and represents a straightforward arrangement for realizing a light trapping spectral beam-splitting photovoltaic receiver. The geometry provides a good base to build a highly efficient photovoltaic receiver by minimizing the reflection losses. Reflected sunlight is always directed to the next solar cell inside the assembly. Hence, the architecture provides several absorption possibilities for a wide spectral range. In order to further reduce optical losses, the spectrally selective beam-splitters are placed directly in front of the solar cells. A good optical connection between the glass substrates with filters and the solar cells minimizes reflections and increases the transmission of sunlight into the solar cells. The parallelepiped provides three sites for placing solar cells into the light beam. Thus, the architecture is well suited to realize a triple-junction photovoltaic receiver consisting of three individually designed solar cells. In order to increase the number of p-n junctions it is possible to use monolithic multi-junction solar cells in this arrangement instead of just single-junction solar cells. However, the restriction to single-junction leads to a maximal spectral tolerance of the light trap. Another advantage of the receiver architecture is that the parallelepipeds tessellate so they can be packed next to each other without any loss in volume, which might be interesting in central dish concentrator application. Passive or active cooling can be applied on the rear side of each solar cell. The upper surface of the parallelepiped defines the aperture of the receiver. This area can also be defined by an external aperture frame. It is obvious that the aperture of this non-concentrating receiver is much smaller than the active cell area, which results in reduced irradiance on each individual solar cell, which is further limited by the spectrum-splitting. However, a possible application of the receiver would be to illuminate it with concentrated light through the aperture of the receiver. Concentrated sunlight increases the solar cell voltages and can result in higher efficiencies, as long as the increased series resistances do not overcompensate them by inducing reduced fill factors. The development of a concentrating receiver has to be done and is not discussed in this paper.

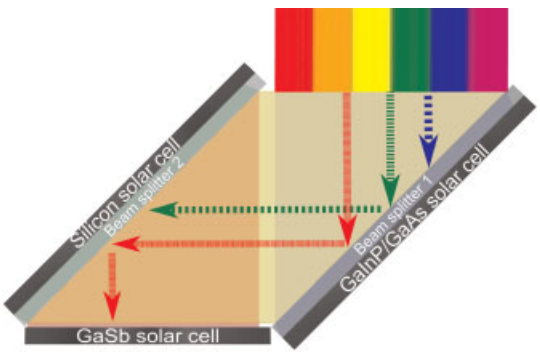

Figure 1. Arrangement of the receiver using the geometry of a 45°-parallelepiped to build a light trapping, spectral beam-splitting architecture including three solar cells and two beam-splitters. The beam-splitters are positioned directly in front of the solar cells and are optically connected with transparent layers of silicone.

3. SOLAR CELLS

The beam-splitting approach allows complete freedom in material selection for each solar cell. Single-junction solar cells as well as monolithic dual-junction solar cells can be used at each surface of the assembly. There are many different types of solar cells which have demonstrated high efficiencies [19]. In order to realize a highly efficient multi-junction receiver, the solar cell system with various band gap energies has to be chosen. Detailed balance calculations [20] using the program code EtaOpt [21] show a global efficiency maximum of 66% for the four-junction beam-splitting receiver with the band gap combination of 2.00, 1.40, 0.95 and 0.50 eV (AM15d ASTM G173-03, 1 MW/m^2). In our setup the solar cells a dual-junction $Ga_{0.51}In_{0.49}P$/GaAs, a Si and a GaSb solar cell were used with a band gap combination of 1.88, 1.43, 1.12 and 0.73 eV. The theoretical efficiency maximum of this band gap combination is 64.4% and therefore less than 2% of absolute value lower than the global maximum.

Figure 2 shows an efficiency limit contour plot of a four-junction beam-splitting system assuming a fixed $Ga_{0.51}In_{0.49}P$/GaAs solar cell and just varying the second and third solar cell in band gap. The contour plot motivates the receiver solar cell selection. The $Ga_{0.51}In_{0.49}P$/GaAs dual-junction solar cell was chosen in order to increase the

Prog. Photovolt: Res. Appl. 2011; **19**:61–72 © 2010 John Wiley & Sons, Ltd.
DOI: 10.1002/pip

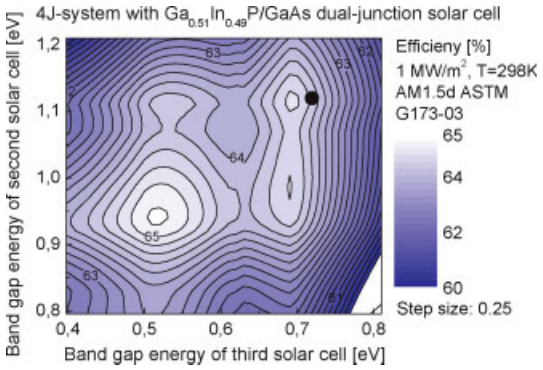

Figure 2. Detailed balance calculations of a four-junction beam-splitting receiver under the AM1.5d ASTM G173-03 spectrum at 1000 kW/m^2 and 298 K. The calculation assumes a fixed $Ga_{0.51}In_{0.49}P$/GaAs top solar cell (1.88 and 1.43 eV) and varies the medium and low band gap sub cells (here second and third solar cell). The black dot indicates our material choice representing a Si and GaSb solar cell (1.12 and 0.73 eV) leading to a receiver theoretical efficiency maximum of 64.4%.

number of p-n junctions of the receiver and represents the most efficient and well-known high band gap solar cell type. Figure 2 is calculated for 1 MW/m^2 irradiation (AM1.5d ASTM G173-03) at 298 K and gives a good basis to select a well-suited combination of band gaps. A high concentration ratio was assumed in order to calculate the efficiency potential of an idealized four-junction beam-splitting receiver. The local maxima do not change their position much by changing the concentration ratio and therefore the same band gaps for the one sun receiver setup can be used. The calculated contour plot, as shown in Figure 2, helped to select the second and third solar cell. A Si solar cell as medium band gap device and a GaSb solar cell as low band gap converter provide a set of band gap materials which have a limiting efficiency close to the global maximum in assembly with the $Ga_{0.51}In_{0.49}P$/GaAs solar cell. The three solar cells were all fabricated at Fraunhofer ISE.

The contour plot also shows three local maxima of efficiency, which is due to the shape of the solar spectrum and to the missing current-matching constraint in the receiver. Low efficiency gradients are shown in the area defined by the band gap range 0.9–1.15 and 0.5–0.7 eV for the second or third solar cell. In this area the limiting efficiency of the receiver stays between 64–65.3% revealing a freedom in material selection. Thus, the beam-splitting receiver provides a window of possible material selections all showing high limiting efficiencies. This is an indication of a low sensitivity to spectral changes, which is an important limiting factor of multi-junction devices under terrestrial operation.

The lateral spectrum splitting is a design to break the current matching restriction. However, the choice of the monolithically series connected $Ga_{0.51}In_{0.49}P$/GaAs dual-junction solar cell induces the current matching restriction again. In order to avoid the restriction completely a single-junction GaInP solar cell can be chosen as high band gap solar cell. Simulations showed that this three junction receiver, incorporation a GaInP, a Si and a GaSb solar cell, has a limiting efficiency of 61.4% (AM15d ASTM G173-03, 1 MW/m^2).

4. BEAM-SPLITTING OPTICS

The key parts of the spectral beam-splitting receiver are the beam-splitter themselves. However, these additional optical elements are sources of losses within the photovoltaic receiver. In order to minimize the losses the absorption of the beam-splitters should be low and its reflectance and transmittance properties have to be close to an ideal step function characteristic as shown in Figure 4.

Our receiver design includes two spectrally selective beam-splitters that divide the solar spectrum into three parts. Firstly, beam-splitter 1 should ideally transmit the sunlight between 300 and 850 nm and reflect the light with higher wavelengths in the region 850–1800 nm. Whereby beam-splitter 2 should ideally transmit the sunlight between 300 and 1080 nm and reflect wavelengths between 1080–1800 nm. These characteristics represent typical short pass filters and are called dichroic mirrors. They consist of stacks made of two materials deposited on a glass substrate. Over two hundred layers of TiO_2 and SiO_2 are used to realize interference systems that demonstrate the required step function characteristics. The dichroic mirror is then connected to the solar cell with the use of a transparent, refractive index matched silicone (Figure 3). The thick dark lines (simulated system) in Figure 4 show the simulated transmittance characteristics of the first and second beam-splitter as they perform in the receiver with the silicone outgoing medium.

An important step was to measure the deposited beam-splitter stacks and verify their characteristics. As it is not possible to measure the transmittance for a beam-splitter in the receiver setup mounted on a solar cell, the transmittance was measured for the beam-splitters on glass substrates without a silicone outgoing medium, here denoted 'single' (Figure 3). The transmittance of the 'single' case has also been simulated for the same beam-splitter stacks. Its measurement differs from the actual case (simulated system), because there is an additional reflection on the backside of the glass substrates due to the air interface, which reduces the transmittance of the total stack.

Figure 4 shows that measurement and simulation of the 'measured' and 'simulated single' stacks are in excellent agreement. It is therefore assumed that the simulated system transmittance is an accurate description of the actual characteristic. It is noted, that the reflection of the solar cell, which is added in the experimental setup, is not included in the simulation of Figure 4. However, by calculating and measuring the solar cell reflectance the whole receiver can be simulated, which has been done for

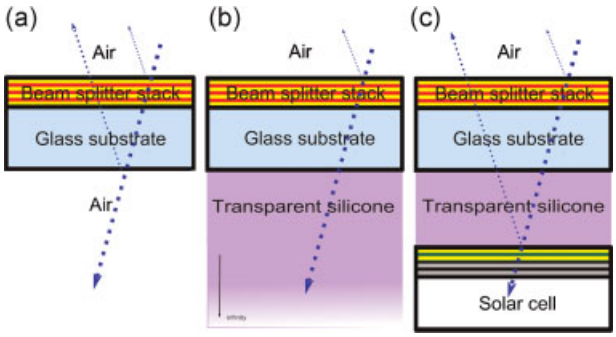

Figure 3. Interface configurations used as basis for the optical simulation of the dichroic mirrors: (a) multilayer stack on a glass substrate with air as ingoing and outgoing medium, denoted 'single'. (b) similar configuration, denoted 'system', in which the refractive indices of the outgoing medium (silicone) and the glass substrate almost match, strongly reducing reflections at the backside interface and (c) actual receiver configuration including an anti-reflection coated solar cell.

the ideal and simulated filter characteristics. The ideal case (step function) was used to calculate the optical efficiency of the receiver prototype, which is covered in more detail in the discussion.

Under these assumptions, the beam-splitters 1 and 2 both transmit 91.7 and 93.8% of the solar spectrum (AM1.5d ASTM G173-03 weighted) in their transmittance bands into the silicone interconnection layer or, assuming a perfect anti-reflection layer, into the solar cell. The spectrally weighted reflectance for the wavelengths above the defined cut-off also reach very high values of 97.5% for beam-splitter 1 and 96.8% for beam-splitter 2.

In order to reach even higher transmittances it is necessary to improve the material and deposition quality. Potential transmittances of up to 96% and reflectances of above 98% were simulated for the same beam-splitter stacks. Necessary features are lower absorption of the TiO2 and reduced scattering.

Non-ideal transmittance and reflectance characteristics of the beam-splitters will lead to voltage and photon loss, respectively, inside the system. A voltage loss occurs when a high energy photon is not absorbed by the optimal solar cell with highest band gap possible, but by a lower band gap solar cell, thus generating a lower photovoltage. This is the case for a non-ideal transmittance ($T < 100\%$) in the transmittance band. Whereas non-ideal reflectance ($R < 100\%$) in the reflection band will result in a photon loss, because transmitted photons with higher wavelength than the absorption edge of the solar cell underneath will not contribute to the photocurrent generation. For instance, the light in the range of 850–1800 nm, which is directed onto the $Ga_{0.51}In_{0.49}P$/GaAs solar cell due to non-ideal reflection of beam-splitter 1, will get lost by means of free carrier absorption or non-ideal reflection of light at the backside mirror of the solar cell. Therefore, it is of high importance to realize an optical design with a high reflectance in the desired reflection range. As can be seen, beam-splitters 1 and 2 show a reflectance of $> 96\%$ which keeps the photon loss low. Another design aspect considers the choice of the cut-off wavelength of the beam-splitters.

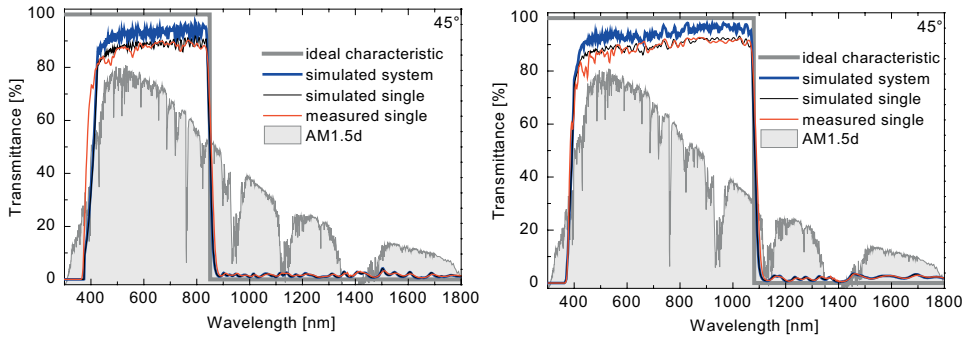

Figure 4. Optical transmittance of beam-splitters 1 and 2 (left and right, respectively) as a function of wavelength with cut-off at 850 (1080) nm. The thick dark lines (simulated system) show the simulated characteristics for a system setup with 45° incidence angle and no solar cell reflectance. They are close to the ideal step function characteristic. The measured transmittances of the fabricated beam-splitters on glass substrate (measured single) are in good agreement with the theoretical simulations (simulated single). The spectrally weighted transmittances of the simulated system characteristics between 410 and 850 (1080) nm are 91.7 (93.8) % (AM1.5d ASTM G173-03) and the weighted reflectances between 850 (1080) and 1800 nm are 97.5 (96.8) %.

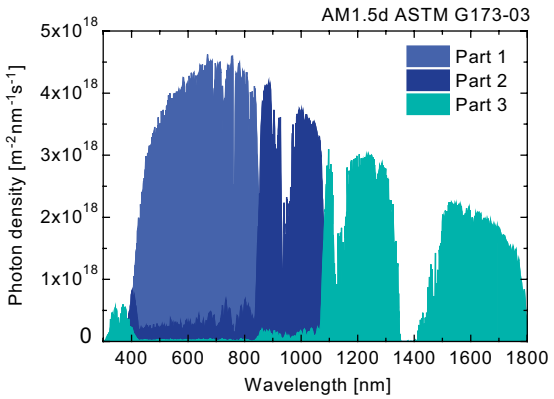

Figure 5. Partial solar spectra of AM1.5d ASTM G173-03 that are directed onto the three different solar cells. The spectra were calculated with the simulated spectral beam-splitter characteristics and solar cell reflectances. Part 1 is directed onto the $Ga_{0.51}In_{0.49}P$/GaAs, part 2 onto the Si, and part 3 onto the GaSb solar cell.

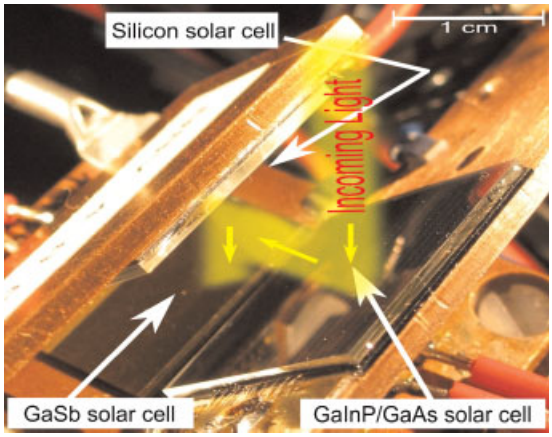

Figure 6. Photograph of the receiver solar cell assembly as experimentally realized. The solar cells of the receiver form a 45°-parallelepiped in which the sunlight is trapped and absorbed by four p-n junctions. As sketched the sunlight first irradiates the filter glass covering the $Ga_{0.51}In_{0.49}P$/GaAs dual-junction solar cell. The reflected part is then directed towards the next dichroic filter with the Si solar cell and finally the uncovered GaSb solar cell located at the bottom of the system. The aperture defining blind was removed to take the photograph.

There is an optimum cut-off wavelength, depending on the external quantum efficiency of the solar cells and open circuit voltages, which minimizes the photon loss. However, the transition from transmittance to reflective behaviour occurs over a range of about 50 nm. It has been modelled that it is optimal to shift the cut-off of the filters to slightly lower (10–20 nm) wavelengths than the absorption cut-off (50% EQE) of the solar cell behind the beam-splitter, in this way limiting the loss of photons, which may not be absorbed.

The dichroic beam-splitters generate three partial spectra which are directed onto the $Ga_{0.51}In_{0.49}P$/GaAs (part 1), the Si (part 2) and the GaSb solar cells (part 3). The photon densities of the partial spectra are plotted in Figure 5 and are calculated based on the AM1.5d ASTM G173-03 standard spectrum by using the simulated filter characteristics (Figure 4) and solar cell reflectances. Partial spectrum 1 contains 44% of the incoming photons (300–1800 nm) and 57% of the solar energy. Therefore, it is most important to achieve a high conversion efficiency of the solar cell in this spectral band. The Si solar cell is irradiated by a smaller partial spectrum containing 24% of the photons (22% of energy). The rest of the photons (32%) are steered onto the GaSb solar cell positioned third inside the assembly (21% of energy).

5. RECEIVER CHARACTERIZATION

In the receiver setup the beam-splitters are optically connected with the solar cells using a thin layer of transparent silicone. The solar cells are electrically connected and put into a measurement setup forming a 45°-parallelepiped. The aperture is defined by a black blind which is manufactured with tolerances better 0.1 mm. Figure 6 shows the receiver solar cell assembly in the experimental setup. The sunlight is firstly directed to the high band gap solar cell in order to reduce optical losses due to the shape of the solar spectrum, which provides the highest energy density around 600 nm and then slowly decreases in intensity to longer wavelength. It is therefore optimal to absorb the low wavelengths part of the spectrum firstly, because every additional interface will add photon and voltage losses.

The spectral beam-splitting solar cell assembly was fully characterized. Firstly, the external quantum efficiency (EQE) of the total system was obtained by using equipment of the Fraunhofer ISE CalLab [22]. The receiver, as shown in Figure 6, was measured in total including the dichroic optics. Each solar cell was measured successively inside the receiver at their respective mounted angles. In summation the total receiver EQE was obtained. Figure 7 shows the EQE of each solar cell as well as the total receiver EQE as measured inside the receiver. The total receiver EQE is about 90% over the 380–1100 nm range and about 75% between 1100–1700 nm. In particular the Si solar cell displays a remarkably high external quantum efficiency of up to 92%, while the $Ga_{0.51}In_{0.49}P$/GaAs solar cell shows about 80% EQE. The Si solar cell also utilizes the reflected light in the range of 380–850 nm, confirming the light trapping effect of the spectral beam-splitting system. Similarly, the GaSb solar cell converts most of the secondly reflected light in the range from 850–1100 nm.

I-V curves of photovoltaic devices can either be measured with sun simulators or under natural sunlight. There are

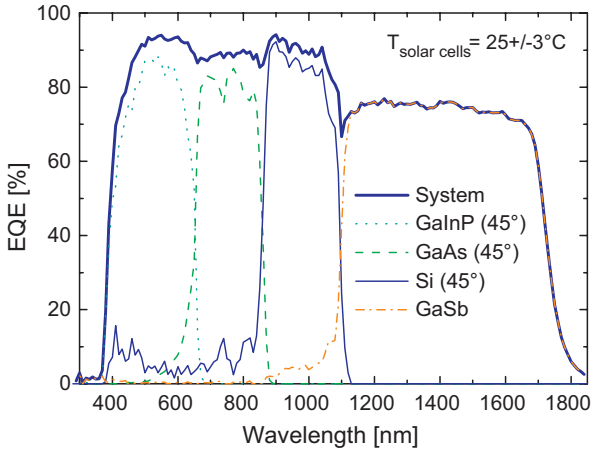

Figure 7. Absolute external quantum efficiencies of the four-junction spectral beam-splitting receiver prototype. Each solar cell was measured successively inside the receiver assembly. The Si solar cell increases the total receiver EQE (addition of all cells) by absorbing the reflected light in the spectral range between 380–850 nm, as does the GaSb solar cell in the range of 850–1100 nm. The $Ga_{0.51}In_{0.49}P$/GaAs and the Si solar cells were measured at their assembled angle of 45° and the GaSb cell at 0°.

several sun simulators available at ISE CalLab suited to measuring different types of solar cells. However, these sun simulators show a light divergence, (multi source sun simulator: $> 10°$, single source sun simulator: $\sim 5°$) and some light would be expected to escape the light trap if the spectral beam-splitting setup were characterized as is without modifications (lateral surface mirrors). Thus, an aperture blind was applied in order to illuminate an area, which is much smaller than the solar cells. This enabled measurement of the individual short circuit currents of the spectral receiver while preventing light spilling due to the divergent sun simulator irradiation. The short circuit current densities of each solar cell under the AM1.5g IEC60904-3Ed2 spectrum with an irradiation of $1000\,W/m^2$ at $25 \pm 3°C$ cell temperature can then be calculated using this measurement and the EQE data for spectral calibration [22]. The determined short circuit current densities, normalized to the receiver aperture area (A_{aa}) are listed in Table I. They are both given for the global and the direct spectra (AM1.5g IEC60904-3Ed2, AM1.5d ASTM G173-03).

The performance of the solar cells under the low intensity caused by the small aperture area and the spectral splitting is lower than under homogenous one sun illumination. A resulting lower fill factor and open circuit voltage reduce the solar cell efficiencies quite drastically, which shows that common sun simulators are not appropriate tools to measure the performance of vertical beam-splitting architectures. However, as long as the short circuit currents are linear, it is possible to measure the individual solar cell current densities as described.

The receiver solar cell I–V curves were also measured at a special module flash simulator for concentrator modules [23]. In contrast to common sun simulators this setup generates collimated light with an angular divergence $< 0.3°$, which is similar to that of natural direct sunlight. This enables the use of a larger aperture area ($A_{aa} = 2.51\,cm^2$) that increases the irradiance by the factor of 3.3. Therefore, the measurements with the module flash simulator setup simulate a one sun aperture illumination leading to a more intense and homogenous illumination of the solar cells without loosing photons via the non-mirrored sides of the parallelepiped. The solar cells were measured separately while mounted in the receiver. The light intensity of the module flash simulator was adjusted in order to generate the same short circuit current densities

Table I. Receiver aperture area (A_{aa}), solar cell areas (A_{cell}) and short circuit current densities (J_{sc}) of the individual solar cells in the receiver prototype measured with the ISE CalLab sun simulators and spectrally calibrated with the EQE data. The aperture area (aa) had to be limited to much smaller than the active solar cell area in order to avoid photon loss due to the divergent light of the common indoor continuous light sun simulators. The irradiation energy is therefore strongly reduced in comparison to the standard conditions (1000 W/m^2), and even further reduced for each individual cell by the spectrum-splitting.

	A_{aa} (cm^2)	A_{cell} (cm^2)	$J_{sc,\ AM1.5g}$ (mA/cm^2_{aa})	$J_{sc,\ AM1.5d}$ (mA/cm^2_{aa})
$Ga_{0.51}In_{0.49}P$/GaAs	0.77	4	12.1	11.8
Silicon	0.77	4	12.1	12.5
GaSb	0.77	2.8	12.8	13.7

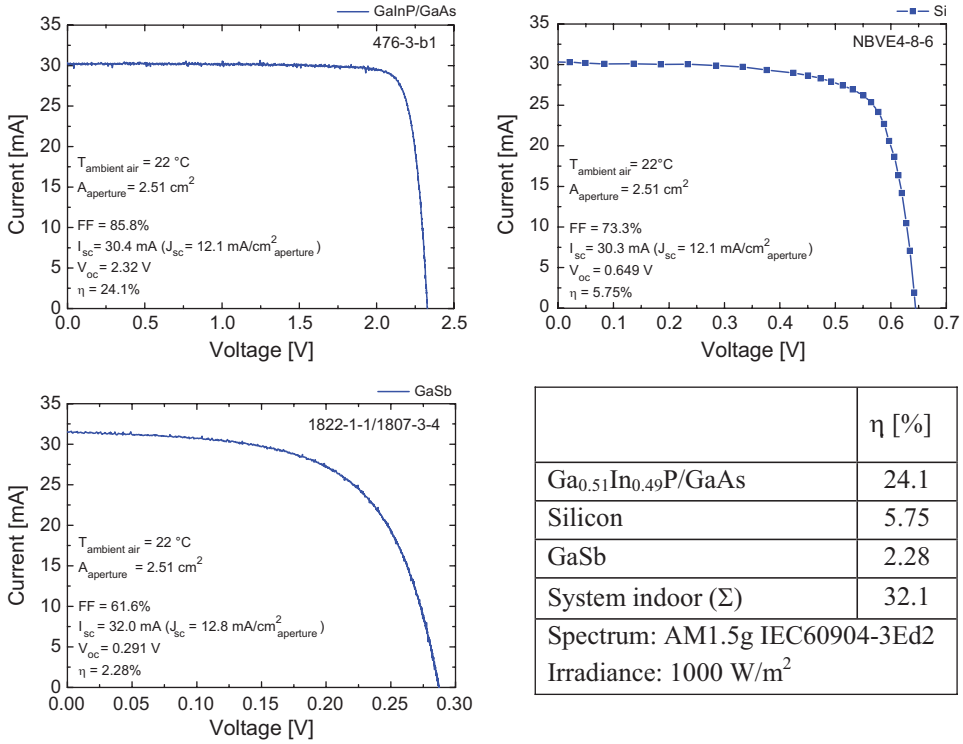

	η [%]
$Ga_{0.51}In_{0.49}P$/GaAs	24.1
Silicon	5.75
GaSb	2.28
System indoor (Σ)	32.1
Spectrum: AM1.5g IEC60904-3Ed2 Irradiance: 1000 W/m^2	

Figure 8. Indoor I-V curves of the three solar cells measured separately while mounted in the receiver assembly with an aperture of 2.51 cm^2 using the concentrator module flash simulator with an intensity of 1000 W/m^2. The $Ga_{0.51}In_{0.49}P$/GaAs solar cell (upper left) shows 24.1% efficiency. The Si solar cell (upper right) was measured in multi flash mode and contributes 5.75% efficiency to the system. Along with the GaSb solar cell (lower left) the total system 1 sun efficiency sums to 32.1% under the AM1.5g IEC60904-3Ed2 spectrum (1000 W/m^2).

as determined under 1000 W/m^2 standard test conditions using the equipment of ISE CalLab. Consequently, the I–V curves of the solar cells were measured at a photocurrent generation corresponding to one sun illumination with the AM1.5g IEC60904-3Ed2 standard spectrum using the independently measured current densities as the reference of the light source. The Si solar cell was measured in multi flash mode due to its high capacitance caused by high lifetime minority carriers. The resulting indoor I–V curves of the receiver solar cells are shown in Figure 8. The $Ga_{0.51}In_{0.49}P$/GaAs solar cell contributes by far the highest portion of the total receiver efficiency. Nevertheless, the Si and GaSb solar cell contribute a substantial part of the total system efficiency pushing it over the current record efficiency under one sun conditions of 32% achieved by a lattice-matched triple-junction $Ga_{0.51}In_{0.49}P$/GaAs/Ge solar cell [24].

The spectral beam-splitting receiver was also measured outdoor in Freiburg, Germany [25–27]. The measurements were taken on the 28th of July, which was a clear and sunny day with high direct normal irradiance. The sun provides parallel light with an opening half-angle of less than 0.3°. The test stand accomplishes measurement of the direct and global normal irradiance (DNI, GNI) with use of an Eppley NIP pyrheliometer (opening angle = ±2.9°) and a Kipp & Zonen pyranometer. The accuracy of both irradiation measurement instruments is specified to be better than 5%. The receiver was covered by a black box to avoid stray light injection. Moreover, a collimator tube (angle of view = 1.7°) was attached in front of the solar cells in order to limit the incident light to direct normal irradiation. The I–V curve was taken in series connection, because the current outdoor measurement equipment was not able to measure the low open circuit voltage of the GaSb solar cell separately, due to the fact that it was designed for concentrator modules. The short circuit currents of all three solar cells inside the receiver are quite similar (Figure 8). Therefore, the measured efficiency reaches up to 34.3% under direct normal irradiance of 863 W/m^2, even if the series connection is due to current matching restriction not the optimal configuration (Figure 9, left). Spectral changes lead to small changes in efficiency, e.g. the red shift of the solar spectrum in the evening induces an increased fill factor, because the current is then limited by the $Ga_{0.51}In_{0.49}P$/GaAs solar cell in series connection with the Si and GaSb solar cells (Figure 9, right).

The beam-splitting receiver reaches its highest photovoltaic conversion efficiency in separate connection of each

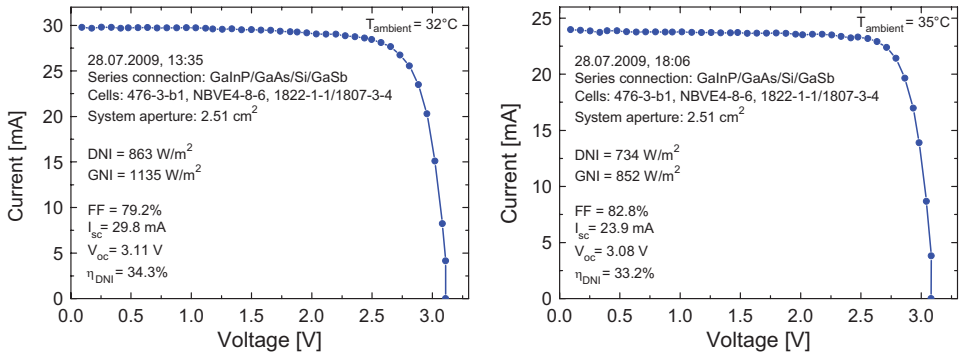

Figure 9. Outdoor I–V curves of the receiver measured in Freiburg, Germany. The three solar cells of the receiver were connected in series and measured with a collimator tube attached. The best measured efficiency is 34.3% (left) normalized to the direct normal irradiance (DNI). The I–V curve shown on the right is measured in the evening. An increased fill factor and a reduced short circuit current (normalized to DNI) were measured because the $Ga_{0.51}In_{0.49}P$/GaAs solar cell was then limiting the current due to red shift in the solar spectrum that is measurable about three hours before sunset.

solar cell as done in the indoor measurements. Future outdoor measurements aim to perform these separate measurements outdoors and even higher efficiencies can be expected.

6. DISCUSSION

The spectral beam-splitting approach increases the system complexity in comparison with a monolithic multi-junction solar cell by adding dichroic optics. The optical efficiency of the system has to be very high. Otherwise, optical losses could overcompensate the gain achieved by the spatial separation of the solar cells. Therefore, the optical efficiency will be discussed in more detail here.

At first, the photon loss occurring from the beam-splitters and the optical interconnection of the beam-splitters and solar cells is investigated. Table II compares the calculated short circuit current densities of an ideal optical system, which assumes ideal filter characteristics and no absorption, with the calculated short circuit current densities of a simulated system and the actual measured short circuit current densities of the receiver. The simulated short circuit currents are accounting the actual dichroic filter characteristics, their absorption losses and the solar cell reflectance, but no additional absorption in the silicone or the substrate glass. The calculations use the simulated filter characteristics, the measured EQE data of the solar cells, their simulated reflectance and the AM1.5g IEC60904-3Ed2 standard spectrum. The short circuit current densities of the receiver were measured with equipment available at ISE CalLab (Figure 8).

There are two main effects visible in Table II. On the one hand, it is possible to quantify the unwanted photon transfer from the upper solar cell ($Ga_{0.51}In_{0.49}P$/GaAs) to the Si solar cell which is ~4.3%. It is defined as the fraction of the transferred photocurrent to Si solar cell of the photocurrent of GaInP/GaAs cell in ideal case and is caused by the non-ideal transmittance band of the dichroic filters and reflections from the solar cell and represents the main loss mechanism of the receiver. The Si solar cell generates a higher short circuit current than in the ideal case because of this photon transfer. Simulation

Table II. Calculated short circuit current densities of a theoretical spectral beam-splitting receiver with ideal optics ($J_{sc,\ ideal}$) compared firstly with the simulated receiver with realized dichroic filters, but no other optical losses ($J_{sc,\ sim}$), and secondly with the at Fraunhofer ISE CalLab measured short circuit current densities of the receiver prototype ($J_{sc,\ proto}$). The non-ideal reflection characteristics and the absorption of the simulated dichroic filters induce a total photon loss of 5.6% (4% characteristics, 1.6% absorption). The actual receiver prototype shows a photon loss of 4.8%. The data refers to the AM1.5g IEC60904-3Ed2 standard spectrum and a receiver aperture area (aa) of 0.77 cm^2.

	$J_{sc,\ ideal}$ (mA/cm^2_{aa})	$J_{sc,\ sim}$ (mA/cm^2_{aa})	$J_{sc,\ proto}$ (mA/cm^2_{aa})
$Ga_{0.51}In_{0.49}P$	14.0	12.2	12.5
GaAs	13.4	12.0	12.1
Silicon	10.9	12.1	12.1
GaSb	13.7	12.8	12.8
System (Σ)	52.0	49.1	49.5

and measurement are in perfect agreement here and a good visualization of this photon transfer is shown in Figure 5.

Summations of the short circuit current densities in Table II reveal that only 5.6% of the receiver photon loss originated from the non-ideal filter characteristic and absorption (column 1→2). The actual receiver measurement (column 3) reveals a photon loss of 4.8% compared to the ideal case. This shows furthermore that the absorption in the silicone layer and the substrate glass of the receiver are negligible.

The photon transfer by reflection leads to another loss mechanism, the voltage loss, which also reduces the system efficiency. Table III quantifies this loss mechanism by calculating the system efficiencies for the same three cases as in Table II. In order to simplify the calculation the changes in fill factor and voltage were neglected. As shown, the ideal optical system leads to an overall receiver efficiency of 34.3% (AM1.5g IEC60904-3Ed2) for the receiver solar cell selection (FF and V_{oc} measured). The actual receiver efficiency is primarily limited by reflections and current limiting losses at and in the $Ga_{0.51}In_{0.49}P$/GaAs solar cell.

The optical efficiency could not be demonstrated experimentally due to the fact that it is not possible to manufacture ideal step function characteristic beam splitters. However, it is calculated to be 93.6% overall. The optical receiver efficiency is defined as the quotient of the receiver prototype efficiency (η_{proto}) and the receiver efficiency with ideal optics (η_{ideal}) (see Table III). The receiver prototype was fully characterized and η_{proto} is a measured value, whereas η_{ideal} was calculated. The calculation assumed ideal step function beam splitter characteristics resulting in partial spectra for each the three solar cells based on the AM1.5g IEC60904-3Ed2 spectrum. The reflectances under the 45° angle were optically simulated in a model with the use of well-known material parameter originating from a large number of 0° incidence measurements and simulations. Furthermore, the EQE data of the single solar cells were taken from standardized 0° measurements [28,29]. The fill factor (FF) and the open circuit voltage (V_{oc}) of each solar cell were measured in the receiver prototype and assumed to be constant for a slight change in irradiation as it takes place in between the ideal, the simulated and the prototype receiver (Table II, Table III).

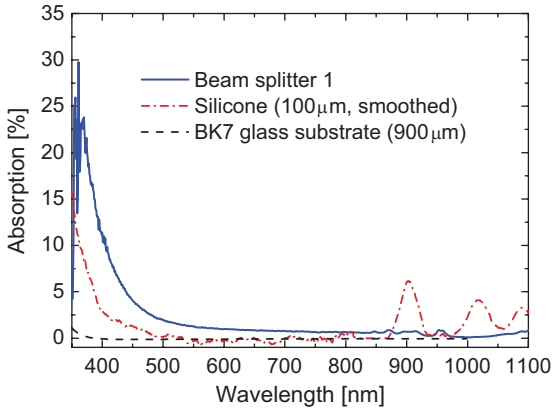

Figure 10. Calculated absorption of the receiver optical system as a function of wavelength. Noticeable absorption occurs between 300–500 nm, mainly induced by the dichroic filters. The silicone causes low absorption between 900 and 1100 nm in particular. The absorption of the BK7 glass substrate is negligible.

As it is shown, the relatively high reflectance at the $Ga_{0.51}In_{0.49}P$/GaAs solar cell induces efficiency losses in particular. This could be improved by an optimized anti-reflection coating taking into account the 45° incident angle and the different refractive index of the incident medium (here silicone instead of air).

The overall absorption of sunlight inside the optical system is not negligible as was shown in Table II. A noteworthy level of absorption occurs in the wavelength range of 300–500 nm (Figure 10), which has an impact on the receiver efficiency in that lowering the photocurrent of the $Ga_{0.51}In_{0.49}P$ solar cell (Table II) by 4.3% relative. Another filter material has been tested to reduce this absorption of the filter, but the successfully lower UV absorption is overcompensated by an undesirable lower reflectance in the reflection band.

Table III. Calculated efficiency of the spectral beam-splitting system (η_{ideal}) with ideal optics (step function characteristics, no absorption) compared with the simulated receiver efficiency with the simulated dichroic filters, but no other optical losses (η_{sim}), and with the measured efficiency of the receiver prototype (η_{proto}). The simulated and the measured receiver solar cell efficiencies are in good agreement, which shows that other optical losses in the receiver setup are negligible. In result, the non-ideal characteristics and the absorption of the manufactured dichroic filter induce a relative efficiency loss of 6.4%. The data refers to the AM1.5g IEC60904-3Ed2 standard spectrum and the EQE of each solar cell and the receiver. The fill factor and the open circuit voltage were assumed to be constant.

	FF (%)	V_{oc} (V)	η_{ideal} (%)	η_{sim} (%)	η_{proto} (%)
$Ga_{0.51}In_{0.49}P$	85.8	2.32	26.7	23.8	24.1
GaAs					
Silicon	73.3	0.65	5.19	5.75	5.75
GaSb	61.6	0.29	2.44	2.27	2.28
System (Σ)			34.3	31.8	32.1

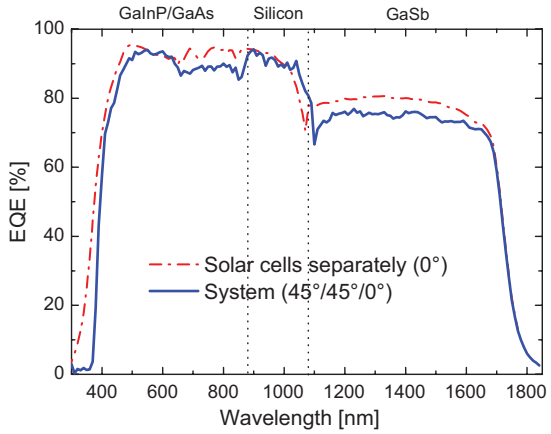

Figure 11. Total external quantum efficiency (EQE) of the receiver in comparison with the EQE of the separate solar cells measured under standard conditions (0°, no filters). The solid line shows the total receiver EQE. The dotted line represents the EQE of the $Ga_{0.51}In_{0.49}P$/GaAs solar cell between 300 and 850 nm, the Si EQE between 850 and 1080 nm and the EQE of the GaSb solar cell in the range of 1080–1850 nm. Absorption reduces the receiver EQE between 300 and 500 nm, whereas a notably high EQE is shown between 900 and 1080 nm. The loss in quantum efficiency at higher wavelength (1080–1800 nm) is caused by non-ideal reflectance of the dichroic filters. The increased receiver EQE at around 1080 nm is due to the light trapping mechanism of the system, which induces that the reflected light is directed towards the GaSb solar cell thereby increasing the total receiver EQE.

Figure 11 discusses the optical losses by comparing the receiver EQE with the individual EQE of the solar cells (added) without filters. Two of the loss mechanisms can be seen in the graph. Firstly, the absorption losses between 300–600 nm are based in the dichroic filters and the silicone. Secondly, the reduced EQE between 1100 and 1700 nm is caused by the non-ideal ($R < 100\%$) reflectance of the spectral beam-splitters, which thereby generates a photon loss in the solar cells due to free carrier absorption and non-ideal infrared reflectance of the solar cell back reflector. The light trapping working principle of the receiver near to the absorption cut-offs of each solar cell can be seen around 1080 nm in particular. The Si solar cell reflectance increases strongly towards 1100 nm due to the single-layer anti-reflection coating. However, the beam-splitter and reflection induced steering of light towards the GaSb solar cell increases the total receiver quantum efficiency between 1000 and 1100 nm to above of the combined individual Si and GaSb quantum efficiencies. Moreover, the receiver EQE is significantly higher in the range of the Si solar cell than at the GaAs range. This is partially caused by the texture of the Si solar cell, and the non-optimized anti-reflection coating of the $Ga_{0.51}In_{0.49}P$/GaAs solar cell. A textured surface is less sensitive to changes in the angle of incidence.

The discussion of the optical efficiency describes the efficiency losses of the receiver as measured indoor. The outdoor measurement shows substantially higher efficiencies, which indicates that the indoor measurements (EQE, IV by common sun simulator) are not the ideal tools to measure vertically expanded photovoltaic devices such as our receiver, even if most of the increase in efficiency is due to the different blue rich spectrum outdoors. It is known that the filter characteristics are angle dependent and especially change to lower transmittance in the transmittance range for higher incidence angles. The lower transmittance at the dichroic filters can be seen in the external quantum efficiency data (Figure 7). The graph shows a lower $Ga_{0.51}In_{0.49}P$/GaAs quantum efficiency than expected, which might be induced due to the divergent irradiation of the receiver during the indoor measurements (besides module flash simulator). Therefore, the total receiver external quantum efficiencies as well as the short circuit currents contain this effect of increased reflectance. Moreover, the short circuit current of the Si solar cell might be non-linear to irradiance especially under strongly reduced irradiation on each solar cell by using an aperture area, which is about four times smaller than the active solar cell area in an additionally spectrum-splitting device. Both effects discussed here indicate a possible underestimation of the measured indoor efficiency.

7. CONCLUSION

This paper shows the modelling and experimentally realization of a spectral beam-splitting system (light trap) containing four p-n junctions and two dichroic beam-splitters. The receiver applies a dual-junction $Ga_{0.51}In_{0.49}P$/GaAs, a Si and a GaSb solar cell, which represent a virtually ideal band gap combination. The experimental results of the receiver are promising, showing conversion efficiencies of up to 34% in outdoor measurements under unconcentrated sunlight. The fabricated dichroic beam-splitters are highly efficient and offer the possibility to build a record efficient photovoltaic receiver. They are used to create a light trapping, photon-recycling geometry, which limits the photon and voltage loss of the spectral splitting. The optical system (filters, interconnection) of the presented spectral beam-splitting receiver only causes a 4.8% loss of photons which leads to a calculated overall optical system efficiency of ~94%, although the utilized solar cells have not been optimized for their usage in the receiver yet. Hence, as the optical system provides low losses the total receiver efficiency is still mostly depended on the solar cells efficiencies itself. However, especially the outdoor measurements indicate the performance potential of the spectral beam-splitting approach. In order to get a better understanding of the indoor measurement methods, simulations of the angle dependence of the system performance have to be done and proven by measurements. Increased transmittances into the solar cells are the key to even higher receiver efficiencies.

Better material quality of the beam-splitter stacks will lead to lower absorption and higher transmittances ($T > 96\%$ simulated).

Moreover, investigations of the receiver performance under concentrated sunlight are necessary to gain a better understanding of the approach and to evaluate the efficiency limit and a possible application of the spectral beam-splitting technology. This has to include simulations and measurements considering the angle dependence of the dichroic beam-splitters as well as optimizing solar cells and geometry of the receiver for the operation under concentrated and divergent sunlight.

ACKNOWLEDGEMENTS

The authors thank Dr Benedikt Bläsi, Armin Bösch, Simon Philipps, Oliver Wolf, Joachim Jaus and Elisabeth Schäffer for their contributions and discussions as well as the whole group 'III-V-epitaxy and solar cells' at Fraunhofer ISE. They also thank Professor E. R. Weber for providing internal Fraunhofer funds for this work.

REFERENCES

1. Fraas LM, Avery JE, Martin J, Sundaram VS, Girard G, Dinh VT, Davenport TM, Yerkes JW, O'Neil VS. Over 35-percent efficient GaAs/GaSb tandem solar cells. *IEEE Transactions on Electron Devices* 1990; **37**(2): 443–449.
2. Gee JM, Virshup GF. A 30%-efficient GaAs/silicon mechanically stacked, multijunction concentrator solar cell. *Proceedings of the 20th IEEE Photovoltaic Specialists Conference*, 1988; 754–758.
3. Wanlass MW, Coutts TJ, Ward JS, Emery KA, Gessert TA, Osterwald CR. Advanced high-efficiency concentrator tandem solar cells. *Proceedings of the 21st IEEE Photovoltaic Specialists Conference*, 1990; 38–45.
4. Guter W, Schoene J, Philipps SP, Steiner M, Siefer G, Wekkeli A, Welser E, Oliva E, Bett AW, Dimroth F. Current-matched triple-junction solar cell reaching 41.1% conversion efficiency under concentrated sunlight. *Applied Physics Letters* 2009; **94**(22): 223501.
5. Garcia I. Rey-Stolle I. Galiana B. Algora C. A 32.6 percent efficient lattice-matched dual-junction solar cell working at 1000 suns. *Applied Physics Letters* 2009; **94**: 053501–053503.
6. Geisz JF, Friedman DJ, Ward JS, Duda A, Olavarria WJ, Moriatry TE, Kiehl JT, Romero MJ, Norman AG, Jones KM. 40.8% efficient inverted triple-junction solar cell with two independently metamorphic junctions. *Applied Physics Letters* 2008; **93**(12): 123501.
7. King RR, Law DC, Edmondson KM, Fetzer CM, Kinsey GS, Yoon H, Sherif RA, Karam NH. 40% efficient metamorphic GaInP/GaInAs/Ge multijunction solar cells. *Applied Physics Letters* 2007; **90**: 183511.
8. Moon RL, James LW, Vander Plas HA, Yep TO, Antypas GA, Chai Y. Multigap solar cell requirements and the performance of AlGaAs and Si cells in concentrated sunlight. *Proceedings of the 13th IEEE Photovoltaic Specialists Conference*, 1978; 859–867.
9. Green MA. Third generation photovoltaics: ultra high conversion efficiency at low cost. *Progress in Photovoltaics: Research and Applications* 2001; **9**(2): 123–135.
10. Marti A, Luque A. Next Generation Photovoltaics: High Efficiency Through Full Spectrum Utilization. Institute of Physics Publishing: Bristol, Great Britain, 2004.
11. Imenes AG, Mills DR. Spectral beam splitting technology for increased conversion efficiency in solar concentrating systems: a review. *Solar Energy Materials and Solar Cells* 2004; **84**(1-4): 19–69.
12. Imenes AG, Buie D, McKenzie D. The design of broadband, wide-angle interference filters for solar concentrating systems. *Solar Energy Materials and Solar Cells* 2006; **90**(11): 1579–1606.
13. Barnett A, Kirkpatrick D, Honsberg C, Moore D, Wanlass M, Emery K, Schwartz R, Bowden S, Aiken D, Gray A, Kurtz S, Kazmerski L, Steiner M, Gray J, Davenport T, Buelow R, Takacs L, Shatz N, Bortz J, Jani O, Goossen K, Kiamilev F, Doolittle A, Ferguson I, Unger B, Schmidt G, Christensen E, Salzman D. Very high efficiency solar cell modules. *Progress in Photovoltaics: Research and Applications* 2009; **17**(1): 75–83.
14. Vincenzi D, Busato A, Stefancich M, Martinelli G. Concentrating PV system based on spectral separation of solar radiation. *Physica Status Solidi A* 2009; **206**(2): 375–378.
15. Fraas LM, Avery JE, Huang HX, Minkin L, Shifman E. Demonstration of a 33% Efficient Cassegrainian Solar module. *Proceedings of the 4th World Conference on Photovoltaic Energy Conversion*, 2006; 679–682.
16. Fraas LM, Avery JE, Strauch J, Girard G. Performance predictions for a Dual Focus Cassegrainian module. *34th IEEE Photovoltaic Specialists Conference*, 2009.
17. Groß B, Peharz G, Siefer G, Peters M, Goldschmidt JC, Steiner M, Guter W, Klinger V, George BM, Dimroth F. Highly efficient light splitting photovoltaic receiver. *Proceedings of the 23rd European Photovoltaic Solar Energy Conference*, 2009; 130–134.
18. Green MA, Ho-Baillie A. Forty three per cent composite split-spectrum concentrator solar cell efficiency. *Progress in Photovoltaics: Research and Applications* 2009; **18**(1): 42–47.
19. Green MA, Emery K, Hishikawa Y, Warta W. Solar cell efficiency tables (version 34). *Progress in Photovoltaics: Research and Applications* 2009; **17**(5): 320–326.
20. Shockley W, Queisser HJ. Detailed balance limit of efficiency of p-n junction solar cells. *Journal of Applied Physics* 1961; **32**(3): 510–519.

21. Létay G, Bett AW. EtaOpt – a program for calculating limiting efficiency and optimum bandgap structure for multi-bandgap solar cells and TPV cells. *Proceedings of the 17th European Photovoltaic Solar Energy Conference*, 2001; 178–181.
22. Meusel M, Adelhelm R, Dimroth F, Bett AW, Warta W. Spectral mismatch correction and spectrometric characterization of monolithic III–V multi-junction solar cells. *Progress in Photovoltaics: Research and Applications* 2002; **10**(4): 243–255.
23. Peharz G, Rodriguez JPF, Siefer G, Bett AW. Indoor characterization of CPV modules at Fraunhofer ISE. *Proceedings of the 5th International Conference on Solar Concentrators*, 2008.
24. Green MA, Emery K, Hishikawa Y, Warta W. Solar cell efficiency tables (version 33). *Progress in Photovoltaics: Research and Applications* 2009; **17**(1): 85–94.
25. Siefer G, Bett AW, Emery K. One year outdoor evaluation of a FLATCON Concentrator module. *Proceedings of the 19th European Photovoltaic Solar Energy Conference*, 2004; 2078–2081.
26. Peharz G, Siefer G, Araki K, Bett AW. Spectrometric outdoor characterization of CPV modules using isotype monitor cells. *Proceedings of the 33rd IEEE PVSC*, 2008; 381–385.
27. Wang X, Waite N, Murcia P, Emery K, Steiner M, Kiamilev F, Goossen K, Honsberg C, Barnett A. Outdoor measurements for high efficiency solar cell assemblies. *Proceedings of the 23rd European Photovoltaic Solar Energy Conference*, 2009; 811–818.
28. Beckert R, Meusel M, Siefer G, Warta W, Bett AW. Determination of absolute external quantum efficiency of monolithic triple-junction solar cells. *Technical Digest of the 12th International Photovoltaic Science and Engineering Conference*, 2001; 577–578.
29. Emery K, Meusel M, Beckert R, Dimroth F, Bett AW, Warta W. Procedures for evaluating multijunction concentrators. *Proceedings of the 28th IEEE Photovoltaic Specialists Conference*, 2000; 1126–1130.